

Hydrothermal synthesis of graphene oxide/multiwalled carbon nanotube/Fe₃O₄ ternary nanocomposite for removal of Cu (II) and methylene blue

Zhihang Long · Yingqing Zhan · Fei Li · Xinyi Wan · Yi He · Chunyan Hou · Hai Hu

Received: 5 April 2017 / Accepted: 31 August 2017 / Published online: 12 September 2017
© Springer Science+Business Media B.V. 2017

Abstract In this work, highly activated graphene oxide/multiwalled carbon nanotube/Fe₃O₄ ternary nanocomposite adsorbent was prepared from a simple hydrothermal route by using ferrous sulfate as precursor. For this purpose, the graphene oxide/multiwalled carbon nanotube architectures were formed through the π - π attractions between them, followed by attaching Fe₃O₄ nanoparticles onto their surface. The structure and composition of as-prepared ternary nanocomposite were characterized by XRD, FTIR, XPS, SEM, TEM, Raman, TGA, and BET. It was found that the resultant porous graphene oxide/multiwalled carbon nanotube/Fe₃O₄ ternary nanocomposite with large surface area could

effectively prevent the π - π stacking interactions between graphene oxide nanosheets and greatly improve sorption sites on the surfaces. Thus, owing to the unique ternary nanocomposite architecture and synergistic effect among various components, as-prepared ternary nanocomposite exhibited high separation efficiency when they were used to remove the Cu (II) and methylene blue from aqueous solutions. Furthermore, the adsorption isotherms of ternary nanocomposite structures for Cu (II) and methylene blue removal fitted the Langmuir isotherm model. This work demonstrated that the graphene oxide/multiwalled carbon nanotube/Fe₃O₄ ternary nanocomposite was promising as an efficient adsorbent for heavy metal ions and organic dye removal from wastewater in low concentration.

Electronic supplementary material The online version of this article (<https://doi.org/10.1007/s11051-017-4014-4>) contains supplementary material, which is available to authorized users.

Z. Long · Y. Zhan (✉) · F. Li · X. Wan · Y. He (✉) · C. Hou · H. Hu
School of Chemistry and Chemical Engineering, Southwest Petroleum University, 8 Xindu Avenue, Chengdu, Sichuan 610500, China
e-mail: zhanyingqing0825@163.com
e-mail: heyi007@163.com

Y. Zhan · Y. He
Oil & Gas Field Applied Chemistry Key Laboratory of Sichuan Province, Southwest Petroleum University, Chengdu, Sichuan 610500, China

Y. Zhan · Y. He
State Key Lab of Oil and Gas Reservoir Geology and Exploitation, Southwest Petroleum University, 8 Xindu Avenue, Chengdu, Sichuan 610500, China

Keywords Graphene oxide carbon nanotubes · Iron oxides · Ternary nanocomposites · Magnetic separation · Methylene blue removal · Cu (II) ion · Adsorption kinetics · Environmental effects · Removal of contaminants

Introduction

Along with the development of industry, wastewater pollution is one of the grimmest problems we are facing today (Cervantes-Avilés et al. 2016). Due to the persistent and non-biodegradable features, heavy metal ions and organic dyes which are often found in industrial wastewaters can be accumulated in living tissues and cause acute toxicity to human beings (Hanif and Shahzad 2014; Xu et al. 2016). Therefore, removal of

undesirable metal ions and dyes from wastewater is of great importance for environment protection. To date, many techniques including bio-leaching, ion exchange, catalytic degradation, chemical precipitation, and membrane filtration have been adopted for removal of contaminants (Molinari et al. 2008; Azarudeen et al. 2014; Costa 2015; Ma et al. 2015; Wu et al. 2016; Yang et al. 2016). Although some achievements were made, the present technologies still fail to meet the requirements of water quality and environment (Schwarzenbach et al. 2006). Recently, adsorption has attracted much attention and become a major technique to remove toxic contaminant from wastewater, due to its great flexibility in design and operation, effective removal for contaminants, and easy recycling process (Chen et al. 2016a).

It was well accepted that the removal efficiency of absorbent is strongly dependent on its surface area, active sites, and adsorption kinetics. Therefore, the traditional adsorbents such as activated carbon dissatisfy the need of water treatment due to the low adsorption efficiency and difficulty to modify ash content which will lead to secondary pollution (Ai et al. 2011b; Fu and Wang 2011). However, the ternary nanocomposites can achieve high adsorption efficiency by combining the advantages of every component. Moreover, the ternary nanocomposites are easier to obtain multifunction compared to single component, which show promising candidates as adsorbents. In recent years, many researchers are dedicating to preparing multifunctional nano-adsorbents to address the shortcomings of conventional adsorbents. For this purpose, many carbon nanomaterials including zero-dimensional (0D) fullerene (Hu et al. 2008), one-dimensional (1D) carbon nanotube (CNT) (Wang et al. 2007; Deb et al. 2011; He et al. 2015), and two-dimensional (2D) graphene (Wei et al. 2012; Yao et al. 2014; Chen et al. 2016b) were applied to prepare new ternary nanocomposites, which intrigued the technological innovation in the enhancement of adsorption efficiency for wastewater.

Graphene oxide, with two-dimensional structure, has been widely applied in energy storage, sensors, catalysis, and environmental science (Gui et al. 2010; Xu et al. 2010; Ghosh and Lee 2012; Huang et al. 2012). Therefore, graphene oxide can be a desirable candidate as adsorbent for removing contaminants from wastewater. To overcome the problem of recycling difficulties, iron oxides were embedded on graphene oxide to achieve magnetic separation (Hu et al. 2013; Santhosh et al. 2014; McCoy et al. 2015; Pucek et al. 2015). The

combination of iron oxide nanoparticles and graphene oxide is cost-effective and has large surface area. Nonetheless, easy aggregation in aqueous solutions and reduction of the sorption sites on carbon surfaces became the major shortcomings for graphene/iron oxide system, which restricted the practical applications. Therefore, anti-aggregation and additional surfaces are required to achieve good adsorption. For this purpose, preparation of ternary nanocomposite architectures composed of CNTs, graphene oxides, and iron oxides was proposed. For example, Il-Kwon Oh and co-workers reported that the 3D graphene-CNTs-iron oxide structures were formed by one-pot microwave method (Vadahanambi et al. 2013). Wang and co-workers reported the one-pot pyrolysis of three-dimensional graphene@carbon nanotube structure by using urea as carbon source (Wang et al. 2015). Although ternary graphene oxide/CNTs nanostructures are proven to be ideal substrates to support iron oxide nanoparticles, the development of facile and dependable synthetic strategies to synthesize structure-controlled, highly efficient, and recyclable adsorbents is still a challenge.

Herein, we report an effective and facile hydrothermal method to prepare graphene oxide/MWCNTs/ Fe_3O_4 (GCF) ternary nanocomposites with high specific surface area and enhanced basal spacing between graphene oxide nanosheets. For this purpose, Fe_3O_4 nanoparticles were used as spacers to prevent the stacking of graphene oxide nanosheets. As a result, it would inhibit the self-aggregation of active metallic oxide nanoparticles (Li et al. 2011; Zhu et al. 2011; Bhaskar et al. 2012; Nam et al. 2013). Furthermore, the large surface area of Fe_3O_4 is a huge advantage for adsorption material. Owing to the unique ternary hybrid architectures and synergistic effect between different components, as-prepared ternary nanocomposites exhibited high separation efficiency when they were used to remove sub-ppm concentrations of Cu (II) and methylene blue from aqueous solutions.

Experimental section

Materials

Natural graphite powder and carboxylated MWCNTs were provided by Chengdu Organic Chemistry limited company of Chinese Academy of Sciences. Concentrated sulfuric acid (H_2SO_4 , 98%), phosphate acid (H_3PO_4),

potassium permanganate (KMnO_4), sodium nitrate (NaNO_3), hydrogen peroxide aqueous solution (H_2O_2 , 30%), anhydrous ethanol (analytical reagent grade), hydrochloric acid (HCl), urea ($\text{CH}_4\text{N}_2\text{O}$), ferrous sulfate heptahydrate ($\text{FeSO}_4 \cdot 7\text{H}_2\text{O}$), copper sulfate pentahydrate ($\text{CuSO}_4 \cdot 5\text{H}_2\text{O}$), methylene blue (MB), and sodium hydroxide (NaOH) were obtained from Chengdu Kelong Chemical Reagent Factory.

Preparation of GCF hybrid structures

GO was prepared by a modified Hummers method (Hummers and Offeman 1958). The GCFs were synthesized by a one-pot hydrothermal method. Typically, 40 mg carboxylated MWCNTs was added into the 40 ml GO aqueous dispersion (2 mg ml^{-1}) to form graphene oxide/MWCNTs framework (GO:MWCNTs = 2:1). After mixing for 30 min, 1.39 g $\text{FeSO}_4 \cdot 7\text{H}_2\text{O}$ was added into the GO/MWCNTs dispersion. Meanwhile, 5 ml NaOH solution (0.2 M) was gradually added. After that, the reaction mixture was stirred at room temperature for 1 h, followed by adding 3.2 g urea. Thereafter, the mixture was sealed in a 100 ml Teflon-lined autoclave and placed inside a preheated oven at $180 \text{ }^\circ\text{C}$ for 12 h for the hydrothermal reaction. The autoclave was cooled to ambient temperature and the product of GCF was separated under magnetic field. After washing with deionized water and ethanol for three times, the sample was dried in a vacuum oven at $60 \text{ }^\circ\text{C}$ for 24 h. As-prepared product was marked as GCF1 and the other two compositions were prepared by varying the amount of graphene oxide/MWCNTs framework and iron source with the same procedure. The amount of graphene oxide/MWCNTs framework, where the ratio of GO:MWCNTs was fixed to 2:1, were 60 mg GCF2 and 180 mg GCF3, respectively. Meanwhile, the amount of iron source was maintained at 1.39 g for GCF2 and GCF3.

Characterization

XRD analysis was carried out by using X'Pert Pro diffractometer (PANalytical, the Netherlands) with copper $\text{K}\alpha$ radiation source. The morphology and structure of products were characterized by scanning electronic microscopy (SEM, JSM-7500F, JEOL, Tokyo, Japan) and transmission electron microscope (TEM, FEI, Tecnai G20). The functional groups of samples were

characterized by fourier-transform infrared (FT-IR, WQF-520, China) spectrophotometer with KBr pellets as the sample matrix Thermogravimetric analyzer (TGA) was recorded on TGA/SDTA851 (METTLER, Switzerland) in the range of $25\text{--}800 \text{ }^\circ\text{C}$. X-ray photoelectron spectroscopy (XPS) was performed on Escalab 250Xi X-ray photon-electron spectrometer (KRATOS, XSAM800). Brunauer–Emmett–Teller (BET) surface area measurement was calculated by Quadrasorb SI-MP (Quantachrome, USA) through N_2 adsorption at 77 K. Measurement was performed in the range of relative pressure from 0.0052 to 0.996. The concentration of Cu (II) solution was tested by atomic absorption spectrophotometer (EWAI, AA-7020). The concentration of methylene blue solution was tested by UV–vis spectroscopy (Shanghai Precision Scientific Instrument Co., UV-762). The size of adsorbents was tested by dynamic light scattering (DLS, BI-200SM, USA). The elements of adsorbed adsorbents were tested by energy dispersive spectrometer (EDS, JSM-7500F, JEOL, Tokyo, Japan). Magnetic curve was obtained by a vibrating sample magnetometer (VSM, Riken Denshi, BHV-525).

Adsorption experiments

Adsorption experiments with different initial concentration

The adsorption capacity of adsorbents (GF and GCFs) was studied by analyzing the concentration of Cu (II) and methylene blue before and after adsorption. The adsorption experiments with different initial concentrations were proceeded at room temperature ($T = 25 \pm 1 \text{ }^\circ\text{C}$) and at a constant pH value (7.0). Twenty five milligrams of adsorbents were added into 50 ml contaminant solution with different concentrations of Cu (II) (1, 4, 7, 10, 13, 16, 19, 22, and 25 ppm) or methylene blue (10, 20, 30, 40, 50, 60, 70, 80, and 90 ppm) in 100 ml conical flask. After stirring for 24 h, the solid phase was separated from liquid phase under magnetic field. The amount of Cu (II) or methylene blue adsorbed by GF and GCFs can be calculated through the initial concentration (C_0) and equilibrium concentration (C_e).

Adsorption experiments with different solution pH

To investigate the influence of solution pH on the adsorption of Cu (II) and methylene blue, 0.5 g/L adsorbents were dispersed into a 50 ml Cu (II) solution

(15 ppm) or methylene blue solution (50 ppm) at various pH values (2–9 for Cu (II) and 2–11 for MB), followed by stirring at room temperature for 24 h.

Adsorption experiments with different temperatures

The adsorption experiments with different temperatures were conducted by varying the operating temperatures (298, 308, 318, and 328 K). Meanwhile, the pH values of Cu (II) and methylene blue solutions were adjusted to 7. The concentration of adsorbents was also 0.5 g/L.

Reusability experiments

After the adsorption of Cu (II), the hybrid materials could be recycled by washing with 100 mL of 0.2 mol L⁻¹ NaOH solution, followed by filtering and drying at 60 °C. And the ethanol as washing agent was used for these hybrid materials' recycle testing after the methylene blue adsorption. Three cycles of all adsorption experiments were needed for the evidence of repeatability. All of the adsorption experiments were repeated for three cycles to assess the reusability.

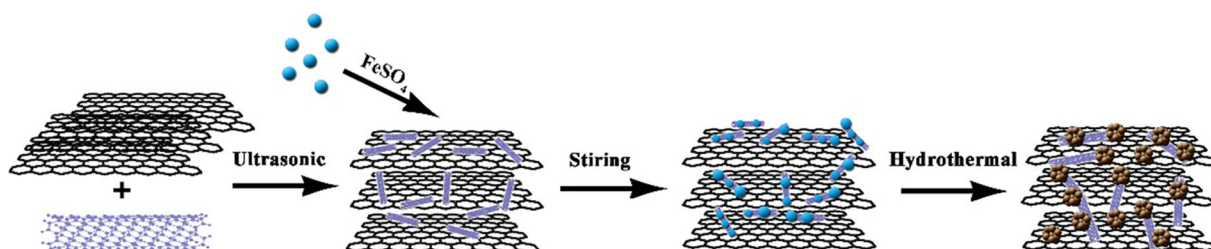
Results and discussion

The synthetic procedure of graphene oxide/MWCNTs/Fe₃O₄ ternary nanocomposite is described in Scheme 1. First, a homogeneous suspension of graphene oxide/MWCNTs was produced by sonication. Due to the presence of π - π attractions, the carboxylated MWCNTs were well dispersed in amphiphilic GO solution after self-assembly, thus forming a porous, crumpled, and loose hierarchical architecture (Yang et al. 2011; Liu et al. 2013). The introduced MWCNTs not only provided oxygen-containing functional groups, but also intercalated layers of GO. By this way, MWCNTs efficiently increased the basal spacing and enlarged the surface area

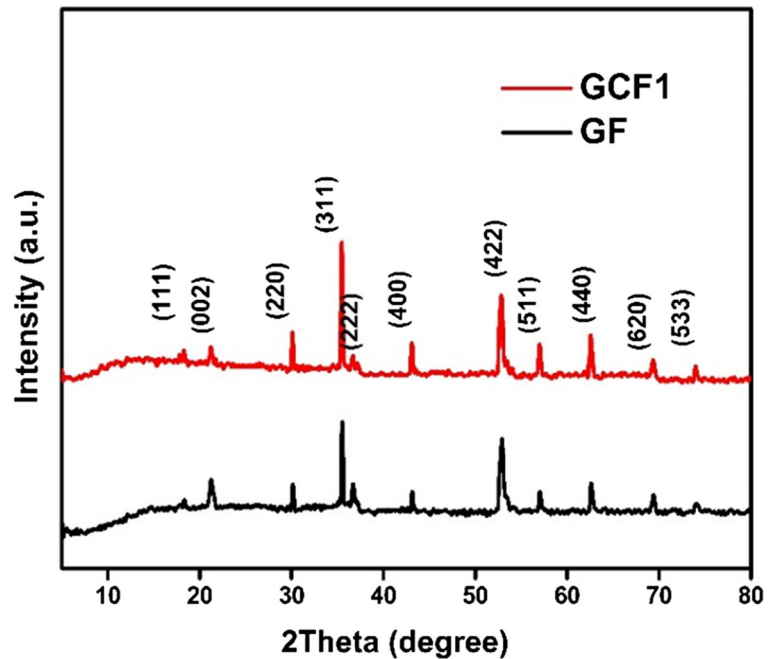
of GO nanosheets which exposed more active sites for contaminant adsorption. Then, FeSO₄·7H₂O was added and formed a stable mixture. The graphene oxide/MWCNTs structures with negatively charged oxygen functionalities (such as -COO⁻ and -OH⁻) could adsorb the positively charged Fe²⁺ through electrostatic attraction (Xiong et al. 2012). During this procedure, OH⁻ provided by NaOH could combine with Fe²⁺ to obtain Fe(OH)₂, followed by transforming into Fe(OH)₃ by oxidation in air. Subsequently, the reaction between CH₄N₂O and Fe(OH)₃ was induced under hydrothermal condition, where CH₄N₂O acted as the reductant in alkaline medium (Yuan et al. 2012). During reaction procedure, Fe₃O₄ nanoparticles which was confined by GO and CNTs in local interspace evolved into porous microspheres gradually due to the Ostwald ripening process (Wan et al. 2007).

XRD patterns of GF and GCF1 are shown in Fig. 1. The (002) plan observed at the diffraction peak of GCF1 corresponded to the GO/CNTs hybrid framework (Zhang et al. 2014). Compared with GF, the (002) peak of graphene was reduced obviously in GCF1, which suggested the decrease of layer stacking. This result demonstrated that a large proportion of graphene oxide sheets were separated by MWCNTs. Moreover, all the characteristic peaks of Fe₃O₄ particles at 2 θ = 18.48°, 30.13°, 35.40°, 36.78°, 43.17°, 53.00°, 57.13°, 62.62°, 69.49°, and 74.06° assigned to the (111), (220), (311), (222), (400), (422), (511), (440), (620), and (533) crystal planes were observed in the diffraction of both two samples. These crystal planes were corresponded to the typical cubic crystal structure of Fe₃O₄. As a result, it indicated that Fe₃O₄ particles were loaded on these ternary GO/MWCNTs frameworks.

To acquire more insights into the structural change of ternary hybrids, the Raman spectra were employed. As shown in Fig. 2, the D bond at 1301 cm⁻¹ and G bond at 1588 cm⁻¹ were ascribed to the disordered and highly ordered graphite, respectively. The I_D/I_G ratios of GF



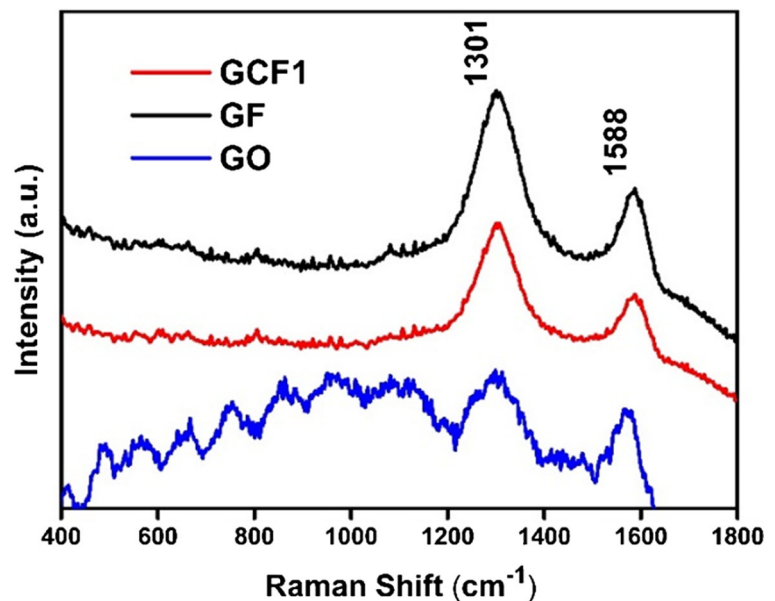
Scheme 1 Synthetic procedure of graphene oxide/MWCNTs/Fe₃O₄ ternary nanocomposite

Fig. 1 XRD patterns of GF and GCF1

and GCF1 (1.26) both were much higher than GO (1.13). The insertion of oxygen-containing groups led to the presence of defects in graphitic plane. Therefore, the increase of I_D/I_G ratios for ternary hybrids was due to the enhancement of oxygen functional group content. However, GCF1, GCF2, and GCF3 showed the same structure which could be observed in Fig. S1. The I_D/I_G ratios of all GCFs ternary hybrids were 1.26, which indicated that these hybrids had the same carbon

structure and the content of Fe_3O_4 would not affect the GCFs hybrids.

The morphology of GF and GCF1 was characterized by SEM (Fig. 3) and TEM (Fig. 4). Figure 3a revealed an interconnected ternary GO/MWCNTs macropore framework in micrometer size. Owing to the existence of π - π stacking, the pore walls were composed by layer stacking of GO sheets. The typical SEM images of GF and GCF1 are depicted in Fig. 3b, c and d, e,

Fig. 2 Raman spectra of pure GO, GF, and GCF1

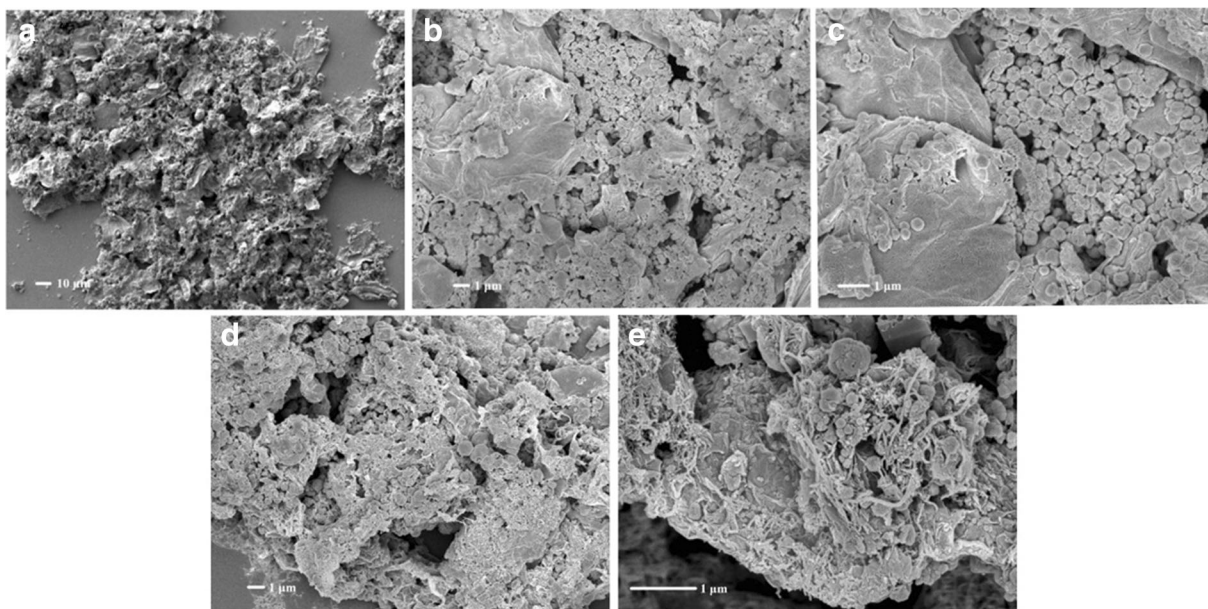


Fig. 3 a SEM image of GCF1 with low magnification ($\times 500$). b, c SEM images of GF with high magnification ($\times 5000$ and $\times 10,000$). d, e SEM images of GCF1 with high magnification ($\times 5000$ and $\times 20,000$)

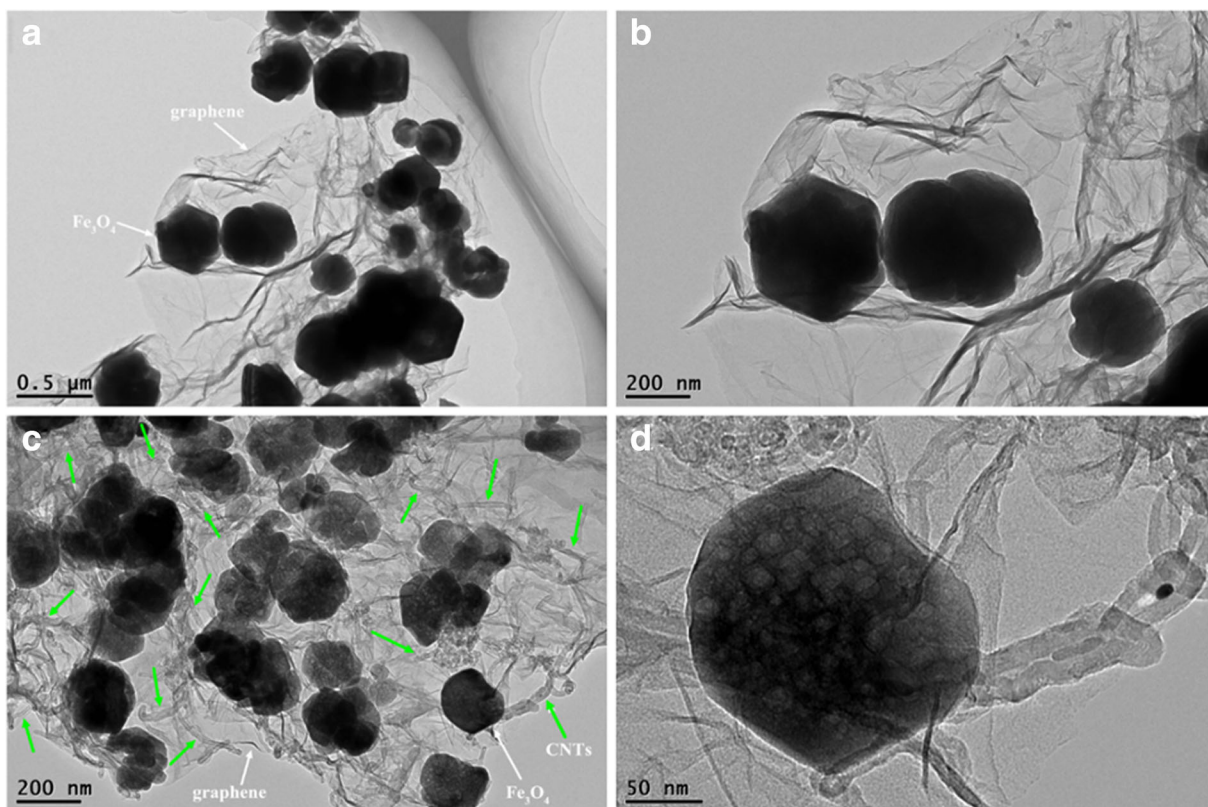
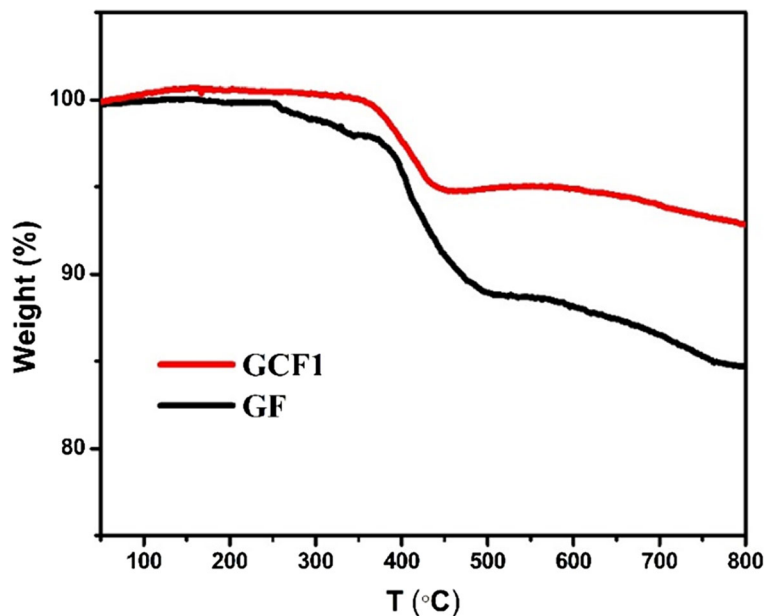


Fig. 4 a-b TEM image of GF. b-c TEM image of GCF1

Fig. 5 TGA curves of GF and GCF1

respectively. By comparing these two samples, it was clear that Fe_3O_4 nanoparticles in GCF1 dispersed more uniformly than that of GF. The notable variation of GCF1 could be attributed to the entangled MWCNTs which twisted around Fe_3O_4 microspheres and interlinked with GO.

TEM images of GF are shown in Fig. 4a, b, in which the Fe_3O_4 nanoparticles were distributed on the GO sheets with a little self-aggregation. However, from the TEM images of GCF1 in Fig. 4c, d, it was clear that GO nanosheets and MWCNTs were interlinked together by Fe_3O_4 nanoparticles. From FTIR spectra (Fig. S2), GF and GCF1 possessed abundant oxygen-containing groups such as $-\text{COO}^-$ and $-\text{OH}^-$. These functional groups would attract ferric ions through electrostatic attraction. Thereafter, the ferric ions would coprecipitate into Fe_3O_4 nanoparticles, which acted as the robust welding point between GO nanosheets and MWCNTs, thus obtaining the interweaved GO/MWCNTs framework (Gao et al. 2015). Typical Fe_3O_4 nanoparticles of GCF1 are shown in Fig. 4a. It was obvious that the average diameter of Fe_3O_4 nanoparticles was around 200 nm. These Fe_3O_4 nanoparticles with porous structures were formed by the aggregation of sub-nanoparticles, as shown in Fig. 4d. Therefore, there was a shell surrounding the interior nanoparticles, which resulted in a rough surface.

TGA was performed on GF and GCF1 to investigate the effect of CNTs on the thermal stability of

hybrid structures, as shown in Fig. 5. From the curve of GF, it was obvious that the weight loss of GF began at 246 °C. The sharp weight loss which occurred at the temperature range 358–509 °C was attributed to the decomposition of oxygen-containing functional groups on GO nanosheets. Also, the major and sharp weight loss in the curve of GCF1 at 356–463 °C was attributed to the same reason. By comparing these two TGA curves, the weight residue of GCF1 was higher than GFs. These results indicated that the introduced CNTs effectively enhanced the thermal stability of hybrid structures.

To confirm the chemical compositions of ternary nanocomposites, XPS survey was carried out. The C 1s spectrum of GF (Fig. 6a) showed four types of carbon bonds including C-C, C = O (carbonyl), C-O (hydroxyl and epoxy), and O-C = O (carboxyl). From the C 1s spectrum of GCF1, the same four types of carbon bonds could be observed (Fig. 6c). However, the content of oxygen functionalities in GCF1 had a clear enhancement compared with GF, which was caused by two aspects. On the one hand, the introduction of carboxylated MWCNTs provided additional oxygen functionalities. On the other hand, the introduced MWCNTs supported the adjacent graphene oxide layers, thus reducing the π - π stacking. These effects increased accessible surface area of graphene oxide nanosheets and led to exposure of more available oxygen-containing groups. Figure 6b

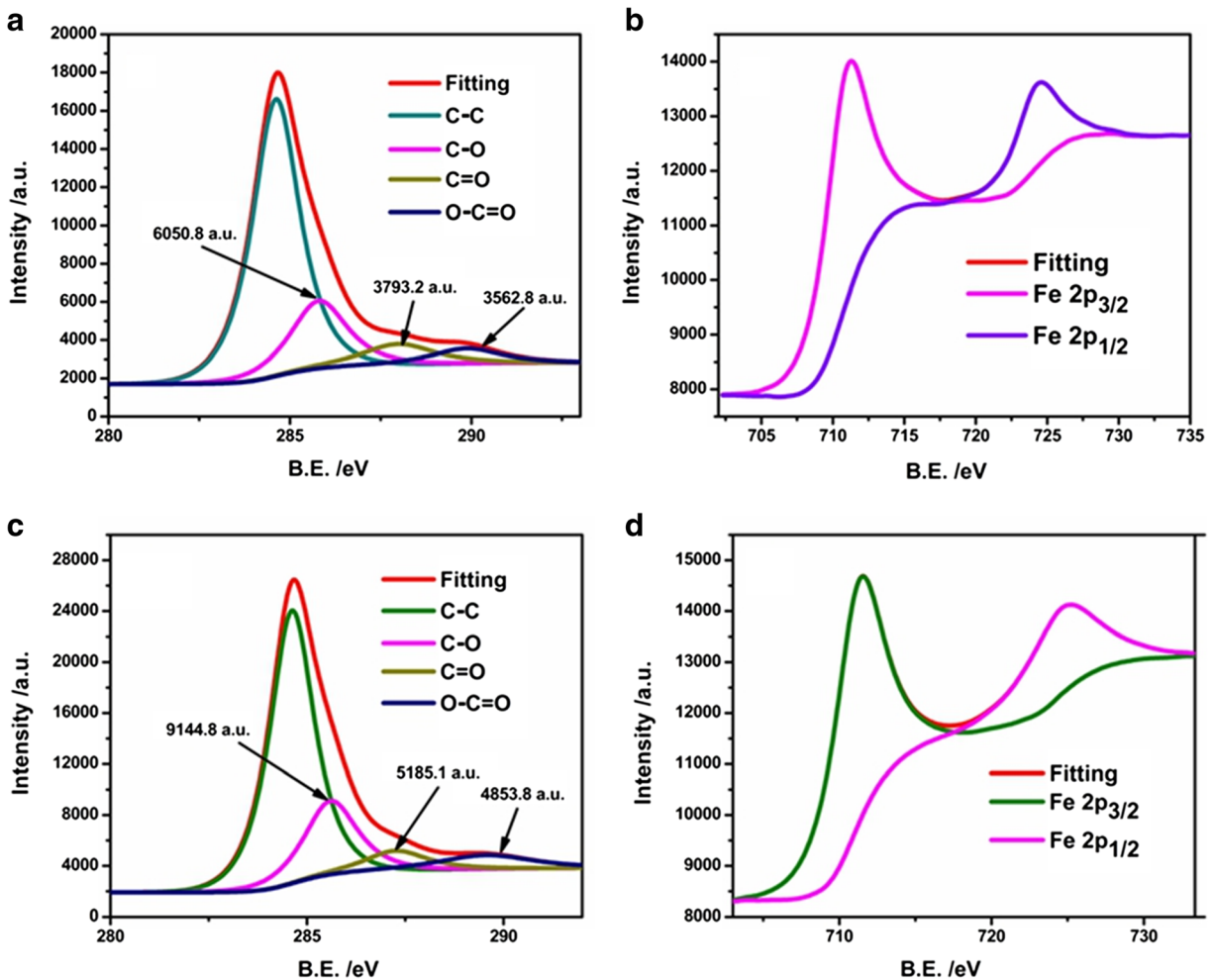


Fig. 6 XPS survey of C 1s core-level spectra for GF **a** and GCF1 **c**. XPS Fe 2p core-level spectra spectrum of GF **b** and GCF1 **d**

shows the Fe 2p spectrum of GF. Two obvious peaks observed at 727 and 712 eV were assigned to the Fe 2p_{1/2} and Fe 2p_{3/2}, respectively. These peaks were in good agreement with Fe₃O₄ phase. By comparing the Fe 2p spectrum of GF and GCF1 (Fig. 6b, d), we concluded that the introduction of MWCNTs had no influence on the crystalline form of Fe₃O₄.

The surface areas of ternary nanocomposites from BET measurement are listed in Table 1. Based on the BET surface area data, the surface area of GCF1 was 102.17 m²/g, which was increased by 24.4% compared with GF. Moreover, the surface area of samples followed the order as GCF3 > GCF1 > GCF2 > GF, which revealed that the incorporation of MWCNTs enhanced the surface area of hybrid architectures. Besides, with the increasing proportion of GO/MWCNTs framework in hybrid structures, the surface

area tended to augment. These results suggested that the surface of ternary framework were occupied by Fe₃O₄ nanoparticles, thus leading to the decrease of surface area.

Ternary composites can integrate the advantages of every component (Fe₃O₄, MWCNTs and GO) and

Table 1 BET results of various GF and GCF hybrids

Samples	BET surface area (m ² g ⁻¹)	BJH desorption pore diameter (nm)
GF	82.18	3.75
GCF1	102.17	3.76
GCF2	93.32	3.78
GCF3	121.16	3.80

exhibit favorable performance. Although these individual components have adsorption ability for Cu (II) or MB (Hao et al. 2010; Sun et al. 2014), their adsorption capacities are low which limited their further application. Binary composites such as CNTs/Fe₃O₄ and GO/Fe₃O₄ exhibited higher adsorption capacity and easy separation from liquid phase compared with the individual components (Yan et al. 2012; Duman et al. 2016). However, their adsorption capacity was limited by aggregation and low-adsorption sites. In contrast, the GCFs ternary nanocomposites were quite distinct from conventional binary structures. Firstly, GO provided abundant adsorption sites and contact areas, which resulted in large surface area. Secondly, the introduction of MWCNTs supported the adjacent GO sheets, which avoided the π-π stacking and led to higher adsorption capacity. Thirdly, the loaded Fe₃O₄ not only interlinked GO nanosheets with MWCNTs, but also acted as the spacers to prevent the restacking of the sheets. In addition, the magnetic Fe₃O₄ would promote the magnetic separation after adsorption. Therefore, GCFs ternary nanocomposites exhibited significant enhancements in adsorption of Cu (II) and MB compared with binary composites.

The experiments of Cu (II) adsorption were carried out to examine the adsorption capacity of ternary nanocomposites. In this work, three different proportions of GCF materials were investigated. The equilibrium adsorption capacity for adsorbents (*q_e*)

could be calculated by the concentrations of Cu (II) before and after the treatment:

$$q_e = \frac{C_0 - C_e}{C_{adsorbent}} = \frac{C_0 - C_e}{m_{adsorbent}} \times V \tag{1}$$

To depict the maximum adsorption capacity of adsorbents, the Langmuir isotherm model was used and expressed as follows:

$$\frac{C_e}{q_e} = \frac{1}{K_L q_{max}} + \frac{C_e}{q_{max}} \tag{2}$$

where *m_{adsorbent}* (g) and *C_{adsorbent}* (mg L⁻¹) represented the mass and concentration of adsorbents GF and GCFs, respectively. *V* represented the volume of aqueous solution (mL), *q_e* was the concentration of Cu (II) adsorbed by adsorbents (mg g⁻¹). *K_L* was the Langmuir constants, which were associated with the adsorption energy (L mg⁻¹). *q_{max}* represented the maximum adsorption capacity of adsorbents (mg g⁻¹).

The adsorption isotherms of four samples are shown in Fig. 7a. From these isotherms, it could be observed that GCF3 had the highest adsorption concentration in all samples and the equilibrium adsorption capacity for adsorbents followed the order GCF3 > GCF1 > GCF2 > GF. To fit the adsorption equilibrium data, the Langmuir isotherm models (Fig. 7b) were applied. Table 2 shows the parameters of Langmuir isotherm model, which indicated the appearance of monolayer adsorption. Besides, the

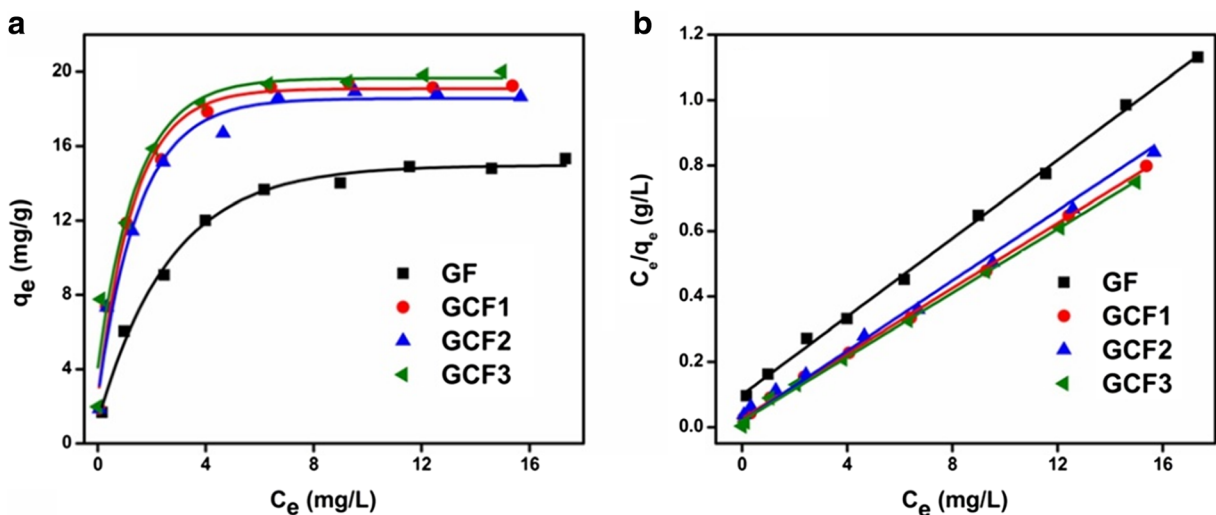


Fig. 7 Adsorption isotherms of Cu (II) (a) and Langmuir isotherms for Cu (II) adsorption (b) on GF, GCF1, GCF2, and GCF3 (room temperature, pH = 7.0, 0.5 g/L adsorbents)

Table 2 Langmuir isotherm model parameters for the adsorption of Cu (II)

Tem (K)	Adsorbent	Langmuir constants		
		q_{\max} (mg g ⁻¹)	K_L (L mg ⁻¹)	R^2
298.15	GF	16.67	0.60	0.9983
298.15	GCF1	20.09	1.87	0.9989
298.15	GCF2	18.66	2.76	0.9979
298.15	GCF3	20.83	2.46	0.9984

weak interactions of adsorbate could be ignored. The maximum adsorption capacity of GF, GCF1, GCF2, and GCF3 for Cu (II) calculated by Langmuir isotherm model were 16.67, 20.09, 18.66, and 20.83 mg g⁻¹, respectively. The maximum adsorption capacity of GCF1 was enhanced by 20.9% compared with GF. These results also demonstrated that the adsorption capacity of ternary nanocomposites followed the sequence mentioned before. It was reported that electrostatic attraction, chemisorption, adsorption, and deposition led to the adsorption capacity of metal ions. In view of this, the existence of active sites (such as -COO⁻ and -OH⁻) on GO (Zhao et al. 2011; Wang and Chen 2015), CNTs (Long and Yang 2001; Wang et al. 2005), and Fe₃O₄ (Kumari et al. 2015) brought about the interaction between Cu (II) and adsorbents. During this electrostatic attraction process, the oxygen-containing functional groups on the nanocomposites as electron donors can coordinate with Cu (II). On the one hand, from the

adsorption data, the adsorption capacity of GCF1 was better than that of GF. These results suggested that introduction of MWCNTs improved the adsorption capacity of ternary nanocomposites. It was attributed to the fact that the presence of MWCNTs enhanced the active sites for Cu (II) adsorption by increasing the basal spacing and enlarging the surface area of graphene oxide sheets. On the other hand, the adsorption capacity of GCFs increased with the proportion of GO/MWCNTs framework in ternary nanocomposites. For instance, the maximum adsorption capacity of GCF3 for Cu (II) was enhanced by 11.6% compared with GCF2, which indicated that the ternary GO/MWCNTs framework played a more important role than Fe₃O₄ in adsorption processes.

Methylene blue, as a usual organic dye, was selected to investigate adsorption capacity of ternary composites for dye. These hybrid materials showed an excellent adsorption capacity for MB. Ten milliliters of MB (15 ppm) could be completely adsorbed by 0.5 g L⁻¹ GCF3, as shown by photo in Fig. 8a. To investigate the adsorption mechanism in detail, the MB adsorption experiment was performed. The adsorption isotherms and Langmuir model are presented in Fig. 8 and the model parameters are shown in Table 3. The q_{\max} values of GF, GCF1, GCF2, and GCF3 calculated by Langmuir model were 45.77, 63.73, 59.48, and 69.40 mg g⁻¹, respectively. The strong interaction between adsorbates and adsorbents led to the high adsorption capacity of MB (Qi et al. 2017). Compared with GF, the adsorption capacity of GCF for MB was enhanced by 39.2%.

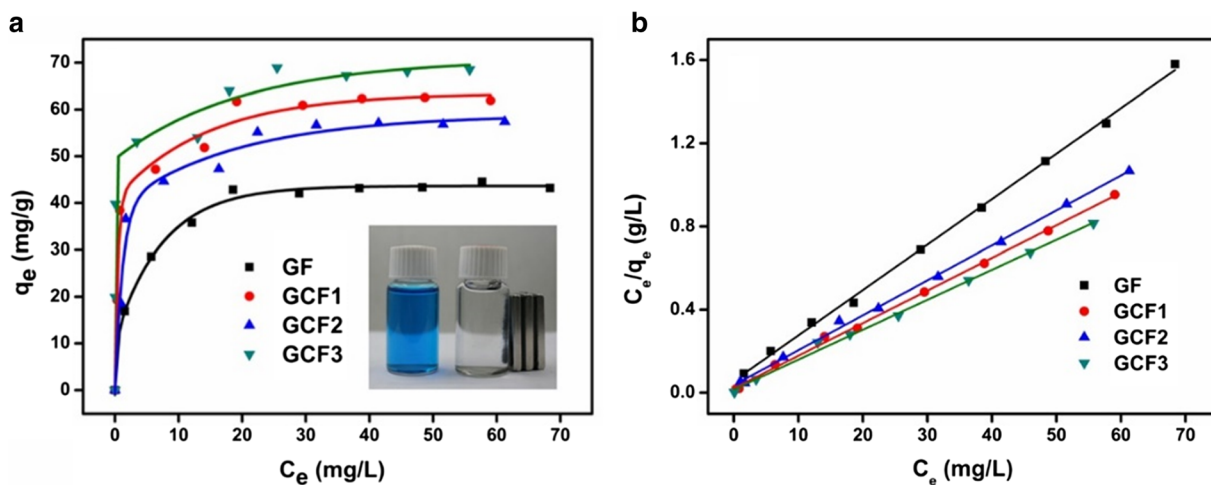
**Fig. 8** Adsorption isotherms of MB (a) and Langmuir isotherms for methylene MB (b) on GF, GCF1, GCF2, and GCF3 (room temperature, pH = 7.0, 0.5 g/L adsorbents)

Table 3 Langmuir isotherm model parameters for the adsorption of methylene blue

Tem (K)	Adsorbent	Langmuir constants		
		q_{max} (mg g ⁻¹)	K_L (L mg ⁻¹)	R^2
298.15	GF	45.77	0.38	0.9984
298.15	GCF1	63.73	0.74	0.9980
298.15	GCF2	59.48	0.46	0.9981
298.15	GCF3	69.40	0.94	0.9966

Moreover, with the increasing of GO/MWCNTs content, the adsorption capacity of GCF3 for MB was 16.7% higher than GCF2. These results were similar to that of Cu (II) adsorption.

The solution pH is one of the important parameters for adsorption of Cu (II) and MB onto the adsorbent. On the one hand, the surface charge and the active sites would be affected by the solution pH. On the other hand, the pH has a great influence on the structure and degree of ionization of MB molecules. Therefore, to investigate the influence of solution pH for adsorption, the adsorption experiments of Cu (II) and MB at different solution pH were conducted. As shown in Fig. 9a, the adsorption capacity of Cu (II) and MB at different pH levels revealed the same tendency. The GCF3 ternary nanocomposite showed a low adsorption capacity at low pH. With the increasing of pH, the adsorption capacity had an obvious enhancement. Methylene blue as the cationic dye is electropositive in solution similar to Cu (II). At low pH, the abundant H⁺ would interact with functional

groups of ternary nanocomposites, which resulted in positively charged adsorbents. In this case, the active adsorption sites for metal ions and cationic dyes would be reduced due to the electrostatic repulsion. With the increase of pH, the surface of GCF3 became negatively charged, thus resulting in high adsorption capacity for cationic contaminants. These results indicated that the electrostatic attraction played an important role in the adsorption process of GCFs ternary nanocomposites. The effect of temperature on adsorption of Cu (II) and MB is presented in Fig. 9b. The adsorption capacity of GCF3 for Cu (II) and MB increased with the increasing of temperature, which demonstrated that these adsorption processes of Cu (II) and MB were endothermal.

As mentioned above, the adsorption of Cu (II) onto the ternary nanocomposite was strongly dependent on the oxygen functionalities. However, the adsorption of MB not only depended on electrostatic attraction, but also lied on the π - π interaction between adsorbent and MB molecules (Zhang and Xu 2014). In most cases, the water waste usually contained various pollutants. Thus, higher requirements for adsorbents are required. In this work, the effect of Cu (II) on the adsorption of methylene blue was carried out to study the co-adsorption behavior of adsorbent, as shown in Fig. 10a. When 10 ppm Cu (II) existed in methylene blue solution, the maximum adsorption capacity of GCF3 for MB was 66.31 mg/g, which was a little bit lower than that of methylene blue solution without Cu (II). Therefore, the Cu (II) adsorbed on the oxygen functionalities would not compete the adsorption sites with MB molecules but could generate new adsorption sites (Wang and Chen 2015). Benzene

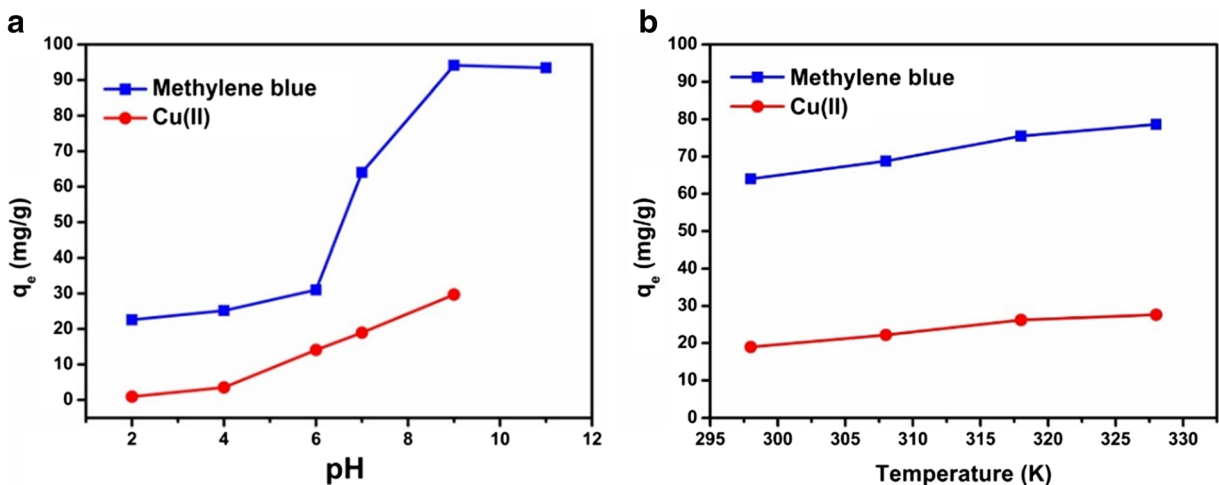


Fig. 9 Effect of pH (a) and temperature (b) on the adsorption performance of GCF3 for Cu (II) and MB

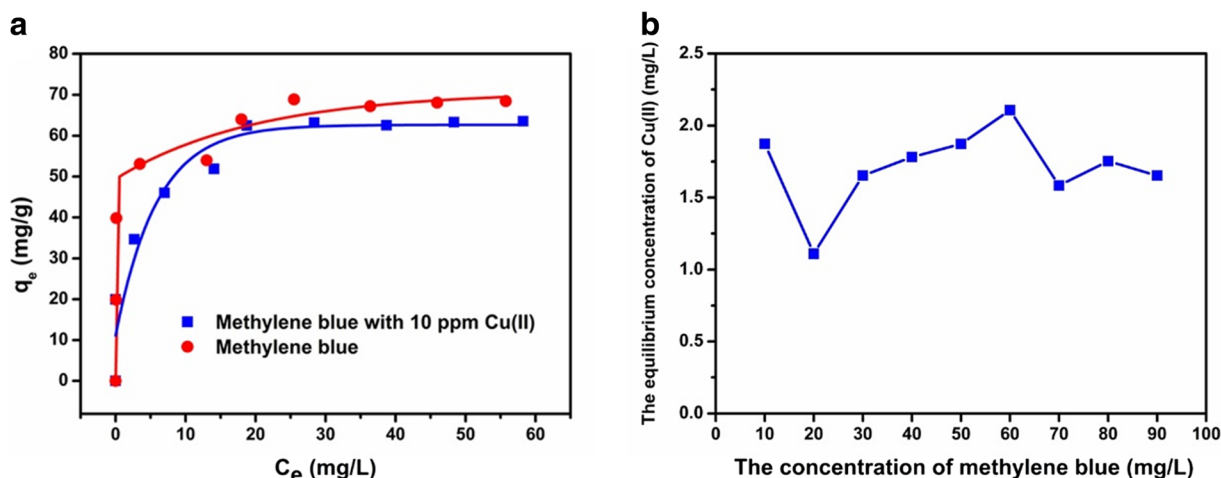


Fig. 10 Adsorption isotherm of MB on GCF3 in the presence and absence of 10 ppm Cu (II) (a), the equilibrium concentration of Cu (II) in various initial concentration of MB after adsorption (b)

ring of MB was π -electron rich donor and showed high affinities for cation adsorption. The Cu (II) adsorbed on the oxygen functionalities could bridge MB and oxidized sites by cation- π interactions. Therefore, the present Cu (II) did not influence the adsorption of MB obviously. Meanwhile, the present Cu (II) was also absorbed in a low concentration (Fig. 10b) as well as in the pure Cu (II) solution. It indicated that the presence of MB molecules in turn would not affect the adsorption of Cu (II). As a result, the GCF ternary nanocomposite could absorb Cu (II) and MB at same time with high adsorption capacity.

To investigate the reusability of ternary nanocomposites for Cu (II) and MB removal, replicated experiments were carried out. The adsorption capacity for Cu (II) and MB both decreased after three cycles, but still maintained at 85.2 and 88.5%, respectively. It suggested that the hybrid materials remained stable after desorption and had favorable reusability. Table 4 shows the comparison of adsorption performance for Cu (II) or MB

among present various binary/ternary and our work. Although our GCF ternary nanocomposite revealed lower adsorption capacity for Cu (II) compared with some other binary/ternary composites, its adsorption capacity for MB remained as high as magnetic cellulose/graphene oxide composite. More importantly, our GCF ternary nanocomposite could adsorb Cu (II) and MB at same time without decline of adsorption capacity. In addition, the GCF ternary nanocomposite was easily separated from solution under external magnetic field, which was beneficial to the cyclic utilization. Therefore, the GCF nanocomposite was ideally absorbent with multifunctional adsorption, high performance, and easy cyclic utilization.

The SEM images of GCF3 after adsorption of Cu (II) and MB are shown in Fig. 11a, b. The structure of ternary nanocomposite was not changed after adsorption. Moreover, the size of GCF3 dispersed in water was tested by DLS at different time intervals (Fig. S3). With

Table 4 Comparison of adsorption performance for Cu (II) or MB among present various binary/ternary and our work

Materials	Contaminant	Q_{max} (mg/g)	Ref.
Chitosan/clinoptilolite nanocomposite	Cu (II)	9.04	(Dinu and Dragan 2010)
Amino-functional Fe_3O_4 /MWCNTs nanocomposite	Cu (II)	30.49	(Zhan et al. 2016)
Sulfonated magnetic graphene oxide nanocomposite	Cu (II)	50.68	(Hu et al. 2013)
Activated carbon/cobalt ferrite/alginate nanocomposite	Methylene blue	33.60	(Ai et al. 2011a)
Magnetic cellulose/graphene oxide nanocomposite	Methylene blue	70.03	(Shi et al. 2014)
GO/MWCNTs/ Fe_3O_4 ternary nanocomposite	Cu (II)	20.83	This work
	Methylene blue	69.40	This work

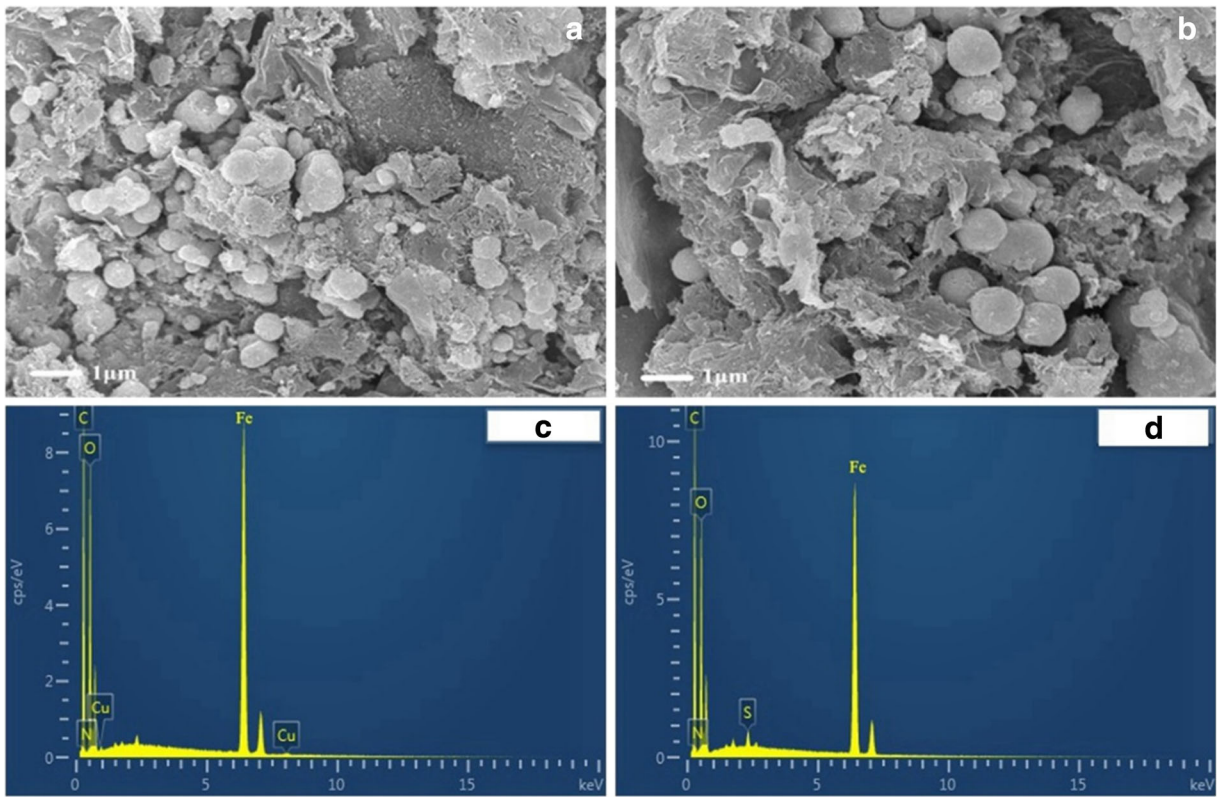


Fig. 11 SEM images of GCF3 after adsorption of Cu (II) (a) and MB (b), EDS spectra of GCF3 after adsorption of Cu (II) (c) and MB (d)

the increasing of dispersion time, aggregation led to a slight size increase of GCF3. Nonetheless, the change of size remained relatively stable during adsorption process. As a result, the structure and morphology of GCFs ternary nanocomposites were stable. After adsorption,

the elements of adsorbents were analyzed by EDS spectra (Fig. 11c, d). The Cu (II) and S elements (from methylene blue) were observed in EDS spectra, which confirmed that the Cu (II) or MB was removed by GCFs ternary nanocomposites after adsorption process.

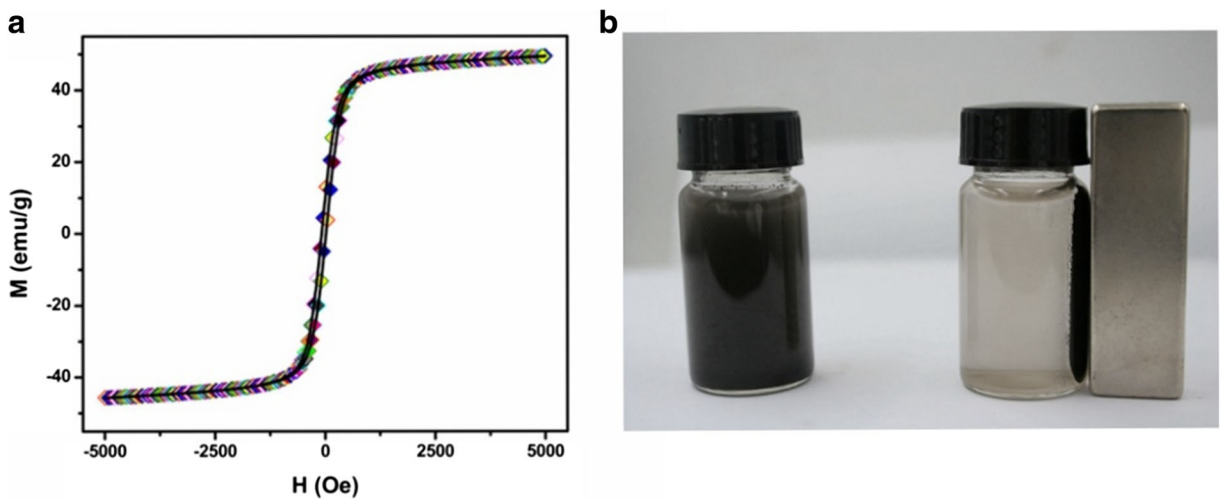


Fig. 12 Magnetization curves of GCF1 at 300 K (a), photograph of GCF1 dispersed in deionized water (left) and separated from liquid phase under magnetic field (right) (b)

A vibrating sample magnetometer was used to investigate the magnetic performance of GCF1, as shown in Fig. 12a. The coercivity and saturation magnetization values were 47.62 Oe and 49.50 emu/g, respectively. These results suggested that the GCF1 hybrid structure had favorable magnetic property. Moreover, Fig. 12b shows that the GCF1 could be separated from liquid phase under magnetic field, which indicated that it was a desired adsorbent for easy cyclic utilization.

Conclusions

In summary, we developed an effective and facile hydrothermal method to prepare graphene oxide/MWCNTs/Fe₃O₄ (GCF) ternary nanocomposites. Such unique architecture not only possessed large surface but also exhibited the desired adsorption capacity for Cu (II) and methylene blue. The adsorption results indicated that the introduced MWCNTs enhanced the adsorption of Cu (II) from 16.67 to 20.09 mg g⁻¹ and the adsorption of methylene blue from 45.77 to 63.73 mg g⁻¹. The sample GCF3 with the high surface area displayed the best adsorption capacity for Cu (II) and methylene blue, up to 20.83 and 69.40 mg g⁻¹, respectively. Furthermore, the resultant GCF ternary nanocomposites exhibited excellent reusability and easy separation under external magnetic field. This work demonstrated that our ternary GCF nanocomposite can be used as promising candidates as absorbents and showed potential application in heavy metal ions and dye removal in wastewater.

Acknowledgements This work was financially supported by Youth Science and Technology Creative Group Fund of Southwest Petroleum University (2015CXTD03) and the Majorly Cultivated Project of Sci-tech Achievements Transition (15CZ0005) from the Education Department in Sichuan Province.

Compliance with ethical standards

Conflict of interest The authors declare that they have no conflict of interest.

References

- Ai L, Li M, Li L (2011b) Adsorption of methylene blue from aqueous solution with activated carbon/cobalt ferrite/alginate composite beads: kinetics, isotherms, and thermodynamics. *J Chem Eng Data* 56(8):3475–3483
- Ai L, Zhang C, Chen Z (2011a) Removal of methylene blue from aqueous solution by a solvothermal-synthesized graphene/magnetite composite. *J Hazard Mater* 192(3):1515–1524
- Azarudeen RS, Ahamed MAR, Subha R, Burkanudeen AR (2014) Heavy and toxic metal ion removal by a novel polymeric ion-exchanger: synthesis, characterization, kinetics and equilibrium studies. *J Chem Technol Biotechnol* 90(12):2170–2179
- Bhaskar A, Deepa M, Rao TN, Varadaraju UV (2012) Enhanced nanoscale conduction capability of a MoO₂/Graphene composite for high performance anodes in lithium ion batteries. *J Power Sources* 216:169–178
- Cervantes-Avilés P, Brito EMS, Duran R, Martínez AB, Cuevas-Rodríguez G (2016) Effect of ZnO nanoparticles in the oxygen uptake during aerobic wastewater treatment. *J Nanopart Res* 18(7):173
- Chen A, Li Y, Yu Y, Li Y, Xia K, Wang Y, Li S (2016a) Synthesis of mesoporous carbon nanospheres for highly efficient adsorption of bulky dye molecules. *J Mater Sci* 51(14):7016–7028
- Chen S, Sun S, Li C, Pittman CU, Lacy TE, Hu S, Gwaltney SR (2016b) Behavior of protruding lateral plane graphene sheets in liquid dodecane: molecular dynamics simulations. *J Nanopart Res* 18(11):317
- Costa CMG (2015) Application of reverse osmosis process associated with EDTA complexation for nickel and copper removal from wastewater. *Desalination & Water Treatment*: 1–9
- Deb AKS, Ilaiyaraja P, Ponraju D, Venkatraman B (2011) Diglycolamide functionalized multi-walled carbon nanotubes for removal of uranium from aqueous solution by adsorption. *J Radioanal Nucl Chem* 291(3):877–883
- Dinu MV, Dragan ES (2010) Evaluation of Cu²⁺, Co²⁺ and Ni²⁺ ions removal from aqueous solution using a novel chitosan/clinoptilolite composite: kinetics and isotherms. *Chem Eng J* 160(1):157–163
- Duman O, Tunc S, Polat TG, Bozoglan BK (2016) Synthesis of magnetic oxidized multiwalled carbon nanotube-kappa-carrageenan-Fe₃O₄ nanocomposite adsorbent and its application in cationic Methylene Blue dye adsorption. *Carbohydr Polym* 147:79–88
- Fu F, Wang Q (2011) Removal of heavy metal ions from wastewaters: a review. *J Environ Manag* 92(3):407–418
- Gao G, Zhang Q, Cheng X-B, Sun R, Shapter JG, Yin T, Cui D (2015) Synthesis of three-dimensional rare-earth ions doped CNTs-GO-Fe₃O₄ hybrid structures using one-pot hydrothermal method. *J Alloys Compd* 649:82–88
- Ghosh A, Lee YH (2012) Carbon-based electrochemical capacitors. *ChemSusChem* 5(3):480–499
- Gui X, Cao A, Wei J, Li H, Jia Y, Li Z, Fan L, Wang K, Zhu H, Wu D (2010) Soft, highly conductive nanotube sponges and composites with controlled compressibility. *ACS Nano* 4(4):2320–2326
- Hanif S, Shahzad A (2014) Removal of chromium(VI) and dye Alizarin Red S (ARS) using polymer-coated iron oxide (Fe₃O₄) magnetic nanoparticles by co-precipitation method. *J Nanopart Res* 16(6):2429
- Hao YM, Man C, Hu ZB (2010) Effective removal of Cu (II) ions from aqueous solution by amino-functionalized magnetic nanoparticles. *J Hazard Mater* 184(1–3):392–399
- He Y, Xu Z, Wu F, Yang Q, Zhang J (2015) Preparation and adsorption studies of β-cyclodextrin grafted onto multi-walled carbon nanotube. *J Chem Technol Biotechnol* 90(12):2257–2264

- Hu X, Liu Y, Wang H, Chen A, Zeng G, Liu S, Guo Y, Hu X, Li T, Wang Y, Zhou L, Liu S (2013) Removal of Cu(II) ions from aqueous solution using sulfonated magnetic graphene oxide composite. *Sep Purif Technol* 108:189–195
- Hu X, Liu J, Mayer P, Jiang G (2008) Impacts of some environmentally relevant parameters on the sorption of polycyclic aromatic hydrocarbons to aqueous suspensions of fullerene. *Environ Toxicol Chem* 27(9):1868–1874
- Huang Y, Liang J, Chen Y (2012) An overview of the applications of graphene-based materials in supercapacitors. *Small* 8(12):1805–1834
- Hummerts WS, Offeman RE (1958) Preparation of graphitic oxide. *J Am Chem Soc* 80(6):1339–1339
- Kumari M, Pittman CU Jr, Mohan D (2015) Heavy metals [chromium (VI) and lead (II)] removal from water using mesoporous magnetite (Fe₃O₄) nanospheres. *J Colloid Interface Sci* 442:120–132
- Li B, Cao H, Shao J, Qu M, Warner JH (2011) Superparamagnetic Fe₃O₄ nanocrystals@graphene composites for energy storage devices. *J Mater Chem* 21(13):5069–5075
- Liu J, Jiang J, Qian D, Tan G, Peng S, Yuan H, Luo D, Wang Q, Liu Y (2013) Facile assembly of a 3D rGO/MWCNTs/Fe₂O₃ ternary composite as the anode material for high-performance lithium ion batteries. *RSC Adv* 3(35):15457–15466
- Long RQ, Yang RT (2001) Carbon nanotubes as superior sorbent for dioxin removal. *J Am Chem Soc* 123(9):2058–2059
- Ma X, Cui W, Yang L, Yang Y, Chen H, Wang K (2015) Efficient biosorption of lead(II) and cadmium(II) ions from aqueous solutions by functionalized cell with intracellular CaCO₃ mineral scaffolds. *Bioresour Technol* 185:70–78
- McCoy TM, Brown P, Eastoe J, Tabor RF (2015) Noncovalent magnetic control and reversible recovery of graphene oxide using iron oxide and magnetic surfactants. *ACS Appl Mater Interfaces* 7(3):2124–2133
- Molinari R, Poerio T, Argurio P (2008) Selective separation of copper(II) and nickel(II) from aqueous media using the complexation-ultrafiltration process. *Chemosphere* 70(3):341–348
- Nam I, Kim ND, Kim G-P, Park J, Yi J (2013) One step preparation of Mn₃O₄/graphene composites for use as an anode in Li ion batteries. *J Power Sources* 244:56–62
- Prucek R, Tuček J, Kolařík J, Hušková I, Filip J, Varma RS, Sharma VK, Zbořil R (2015) Ferrate (VI)-prompted removal of metals in aqueous media: mechanistic delineation of enhanced efficiency via metal entrenchment in magnetic oxides. *Environ Sci Technol* 49(4):2319–2327
- Qi Y, Yang M, Xu W, He S, Men Y (2017) Natural polysaccharides-modified graphene oxide for adsorption of organic dyes from aqueous solutions. *J Colloid Interface Sci* 486:84–96
- Santhosh C, Kollu P, Doshi S, Sharma M, Bahadur D, Vanchinathan MT, Saravanan P, Kim B-S, Grace AN (2014) Adsorption, photodegradation and antibacterial study of graphene-Fe₃O₄ nanocomposite for multipurpose water purification application. *RSC Adv* 4(54):28300–28308
- Schwarzenbach RP, Escher BI, Fenner K, Hofstetter TB, Johnson CA, Von Gunten U, Wehrli B (2006) The challenge of micropollutants in aquatic systems. *Science* 313(5790):1072–1077
- Shi H, Li W, Zhong L, Xu C (2014) Methylene blue adsorption from aqueous solution by magnetic cellulose/graphene oxide composite: equilibrium, kinetics, and thermodynamics. *Ind Eng Chem Res* 53(3):1108–1118
- Sun W, Xia J, Shan Y (2014) Comparison kinetics studies of Cu(II) adsorption by multi-walled carbon nanotubes in homo and heterogeneous systems: effect of nano-SiO₂. *Chem Eng J* 250:119–127
- Vadahanambi S, Lee SH, Kim WJ, Oh IK (2013) Arsenic removal from contaminated water using three-dimensional graphene-carbon nanotube-iron oxide nanostructures. *Environ Sci Technol* 47(18):10510–10517
- Wan J, Cai W, Feng J, Meng X, Liu E (2007) In situ decoration of carbon nanotubes with nearly monodisperse magnetite nanoparticles in liquid polyols. *J Mater Chem* 17(12):1188–1192
- Wang J, Chen B (2015) Adsorption and coadsorption of organic pollutants and a heavy metal by graphene oxide and reduced graphene materials. *Chem Eng J* 281:379–388
- Wang L, Huang Y, Li C, Chen J, Sun X (2015) A facile one-pot method to synthesize a three-dimensional graphene@ carbon nanotube composite as a high-efficiency microwave absorber. *Phys Chem Chem Phys* 17(3):2228–2234
- Wang S, Gong W, Liu X, Yao Y, Gao B, Yue Q (2007) Removal of lead(II) from aqueous solution by adsorption onto manganese oxide-coated carbon nanotubes. *Sep Purif Technol* 58(1):17–23
- Wang X, Chen C, Hu W, Ding A, Xu D, Zhou X (2005) Sorption of 243Am (III) to multiwall carbon nanotubes. *Environmental science & technology* 39(8):2856–2860
- Wei H, Yang W, Xi Q, Chen X (2012) Preparation of Fe₃O₄@graphene oxide core-shell magnetic particles for use in protein adsorption. *Mater Lett* 82:224–226
- Wu J, Ma L, Chen Y, Cheng Y, Liu Y, Zha X (2016) Catalytic ozonation of organic pollutants from bio-treated dyeing and finishing wastewater using recycled waste iron shavings as a catalyst: removal and pathways. *Water Res* 92:140–148
- Xiong QQ, Tu JP, Lu Y, Chen J, Yu YX, Qiao YQ, Wang XL, Gu CD (2012) Synthesis of hierarchical hollow-structured single-crystalline magnetite (Fe₃O₄) microspheres: the highly powerful storage versus lithium as an anode for lithium ion batteries. *J Phys Chem C* 116(10):6495–6502
- Xu P, Niu H, Chen J, Song J, Mao C, Zhang S, Gao Y, Chen C (2016) Facile synthesis of uniform hierarchical composites CuO-CeO₂ for enhanced dye removal. *J Nanopart Res* 18(12):382
- Xu Y, Sheng K, Li C, Shi G (2010) Self-assembled graphene hydrogel via a one-step hydrothermal process. *ACS Nano* 4(7):4324–4330
- Yan L, Chang PR, Zheng P, Ma X (2012) Characterization of magnetic guar gum-grafted carbon nanotubes and the adsorption of the dyes. *Carbohydr Polym* 87(3):1919–1924
- Yang S, Chang K, Tien H, Lee Y, Li S, Wang Y, Wang J, Ma CM, Hu C (2011) Design and tailoring of a hierarchical graphene-carbon nanotube architecture for supercapacitors. *J Mater Chem* 21(7):2374–2380
- Yang X, He Y, Zeng G, Zhan Y, Pan Y, Shi H, Chen Q (2016) Novel hydrophilic PVDF ultrafiltration membranes based on a ZrO₂-multiwalled carbon nanotube hybrid for oil/water separation. *J Mater Sci* 51(19):8965–8976
- Yao Y, Cai Y, Lu F, Wei F, Wang X, Wang S (2014) Magnetic recoverable MnFe₂O₄ and MnFe₂O₄-graphene hybrid as heterogeneous catalysts of peroxymonosulfate activation for efficient degradation of aqueous organic pollutants. *J Hazard Mater* 270:61–70

- Yuan K, Ni Y, Zhang L (2012) Facile hydrothermal synthesis of polyhedral Fe₃O₄ nanocrystals, influencing factors and application in the electrochemical detection of H₂O₂. *J Alloys Compd* 532:10–15
- Zhan Y, Hu H, He Y, Long Z, Wan X, Zeng G (2016) Novel amino-functionalized Fe₃O₄/carboxylic multi-walled carbon nanotubes: one-pot synthesis, characterization and removal for Cu(II). *Russ J Appl Chem* 89(11):1894–1902
- Zhang Z, Xu X (2014) Wrapping carbon nanotubes with poly (sodium 4-styrenesulfonate) for enhanced adsorption of methylene blue and its mechanism. *Chem Eng J* 256:85–92
- Zhang Z, Sun T, Chen C, Xiao F, Gong Z, Wang S (2014) Bifunctional nanocatalyst based on three-dimensional carbon nanotube-graphene hydrogel supported Pd nanoparticles: one-pot synthesis and its catalytic properties. *ACS Appl Mater Interfaces* 6(23):21035–21040
- Zhao G, Li J, Ren X, Chen C, Wang X (2011) Few-layered graphene oxide nanosheets as superior sorbents for heavy metal ion pollution management. *Environ Sci Technol* 45(24):10454–10462
- Zhu X, Zhu Y, Murali S, Stoller MD, Ruoff RS (2011) Nanostructured reduced graphene oxide/Fe₂O₃ composite as a high-performance anode material for lithium ion batteries. *ACS Nano* 5(4):3333–3338